

# Bound-Free Electron-Positron Pair Production in Relativistic Heavy-Ion Collisions

M. Y. Şengül,<sup>1,2,\*</sup> M. C. Güçlü,<sup>1</sup> and S. Fritzsche<sup>3,4</sup>

<sup>1</sup>*Istanbul Technical University, Faculty of Science and Letters, 34469, İstanbul, Turkey*

<sup>2</sup>*Kadir Has University, Faculty of Science and Letters, 34083 Cibali, Fatih-İstanbul, Turkey*

<sup>3</sup>*Department of Physical Sciences, P.O. Box 3000, Fin-90014 University of Oulu, Finland*

<sup>4</sup>*GSI Helmholtzzentrum für Schwerionenforschung, D-64291 Darmstadt, Germany*

(Dated: October 24, 2018)

The bound-free electron-positron pair production is considered for relativistic heavy ion collisions. In particular, cross sections are calculated for the pair production with the simultaneous capture of the electron into the  $1s$  ground state of one of the ions and for energies that are relevant for the Relativistic Heavy Ion Collider (RHIC) and the Large Hadron Colliders (LHC). In the framework of perturbation theory, we applied Monte-Carlo integration techniques to compute the lowest-order Feynman diagrams amplitudes by using Darwin wave functions for the bound states of the electrons and Sommerfeld-Maue wave functions for the continuum states of the positrons. Calculations were performed especially for the collision of  $Au + Au$  at 100 GeV/nucleon and  $Pb + Pb$  at 3400 GeV/nucleon.

PACS numbers: 25.75.Dw; 25.30.Rw

## I. INTRODUCTION

The bound-free electron-positron pair production plays an important role at modern colliders such as the Relativistic Heavy Ion Collider (RHIC) or the Large Hadron Colliders (LHC), since it may restrict the luminosity of the ion beams that will be available. Especially in peripheral collisions of the ions, it is known that a large number of lepton pairs can be produced owing to the Lorentz contracted electromagnetic fields that occur in course of the collisions. In the bound-free pair production, the electron is captured by one of the colliding ions

$$Z_a + Z_b \rightarrow (Z_a + e^-)_{1s_{1/2}, \dots} + Z_b + e^+ \quad (1)$$

and leads to the loss of the (one-electron) ion from the beam. The bound-free pair production (BFPP) will therefore be an important problem at the LHC; in fact, this process does not only reduce the intensity of the beam but also leads to a separate beam of one-electron ions that strikes the beam-pipe about 140 meters away from the interaction point. In the worst scenario, there might be enough energy in this separated beam to quench the LHC magnets as it was first pointed out by Bruce *et al.*[1] but was investigated in further detail in Refs. [2, 3, 4].

A first computation on the bound-free pair production cross sections were performed by Baltz, Rhoades-Brown and Weneser [5] in the mid 1990ies. These authors used large-basis coupled-channel Dirac-equation of BFPP in their calculations. In particular, Baltz and coworkers derived a simple formula for the BFPP cross sections at ultra-relativistic energies ( $\gamma = 23\,000$ )

$$\sigma_{BFPP} = A \ln(\gamma) + B \quad (2)$$

where  $A$  and  $B$  are the parameters independent of energy. In this expression for the cross section, the  $A \ln \gamma$  term represents the region of large impact parameters, and  $A$  was calculated by using perturbation theory, while the parameter  $B$  represents the contributions from small impact parameter and includes both, perturbative and non-perturbative parts. The production of bound-free electron-positron pairs was calculated also by Bertulani and Baur [6] who used a semi-classical method in order to calculate the production of bound-free pairs at energies and for collision systems appropriate for the RHIC facility. From these computations it was found that the BFPP cross sections for the capture of the electron into the  $ns$  excited states of the ion decreases with  $\approx 1/n^3$ , which means a factor of  $1/8$  for the  $L$ -shell and to a net effect of all  $ns$  excited states of approximately 20 % in total [7, 8].

An alternative method was later applied by Rhoades-Brown and coworkers [9] who performed an "exact" integration of the Feynman diagrams by using Monte-Carlo techniques. In this work, the cross section for the capture of an electron was obtained as the convolution of the amplitude of *direct* and *crossed* Feynman diagrams in Fig. 1,

$$B(k, q; \mathbf{p}_\perp) = A^{(+)}(k, q; \mathbf{p}_\perp) + A^{(-)}(k, q; \mathbf{k}_\perp + \mathbf{q}_\perp - \mathbf{p}_\perp), \quad (3)$$

with the momentum distribution of the bound-state wave function. The results from these Feynman-Monte Carlo computations were compared with the Weizsacker-Williams calculations by Baur and Bertulani [6] and were found larger by about a factor of 3, a discrepancy which was explained later in a comment by Baur [10]. In the present work, we have calculated the cross section for the capture of an electron into the  $K$ -shell by applying a Monte-Carlo integration for the lowest-order Feynman diagrams as shown in Fig. 1. This procedure is known also in the literature [11, 12] as the two-photon

\*Electronic address: myilmaz@khas.edu.tr

method since the colliding nuclei (nucleus  $a$  and nucleus  $b$ ) exchange one photon (total two photon) and the two-photon-exchange diagrams are proportional to  $Z\alpha$ . In contrast to our previous computations, where plane-waves were applied for both the electron and the positron [11, 12], we here apply bound  $K$ -shell wave-functions for the electron as well as modified plane-waves functions for the positrons that includes a correction due to the distortion by the ‘bound’ electron. In fact, this distortion of the positron wave function arises from the necessary (re-) normalization of the continuum waves in order to account for the reduction of the wave functions of the positron near to the nucleus to which the electron is localized [13]. In the literature, these (one-particle) functions are known as Sommerfeld-Maue wave functions for the positrons and Darwin wave functions for the bound electrons. Similar wave functions have been applied also in Refs. [6, 13] for studying the captured electrons and free positrons.

In the next section, we first present the formalism for evaluating the pair production cross sections with an electron bound to one of the ions. Apart from the representation of the electron and positron states, this includes the analysis and a step-wise simplification of the bound-free amplitudes by using the wave functions from above. In Section III, then, the differential BFPP cross sections are calculated as function of the transverse and longitudinal momentum, the energy and rapidity, and especially for those collision energies of the ions that are relevant for the RHIC and LHC facilities. A comparison of our Monte Carlo-Feynman calculations with previous computations is made. Finally, a few conclusions are drawn in Section IV.

## II. THEORETICAL BACKGROUND

Lowest-order perturbation theory in the framework of quantum electrodynamics (QED) has been applied to derive and calculate the cross section for generating bound-free electron-positron pairs in relativistic heavy-ion collisions. For this electron-positron BFPP process, the signature is that the electron is captured by one of the colliding ions, while the *free* positron leaves the collision system. In lowest QED order, this process is described by the two Feynman diagrams, the (so-called) *direct* and *crossed* terms, as depicted schematically in Fig. 1. These diagrams represent the leading contributions to the bound-free pair production as appropriate especially for the high collision energies available at the RHIC and LHC facilities.

For two ions  $a$  and  $b$ , that collide with high energy, the leading contributions to the pair production arise from those Feynman diagrams for which each ion interacts exactly once with the electromagnetic field of the other ion. This restriction gives rise to the *direct* and *crossed* diagrams from Fig. 1, and to an gauge-invariant total amplitude that is Lorentz covariant. In the sudden (or impulse)

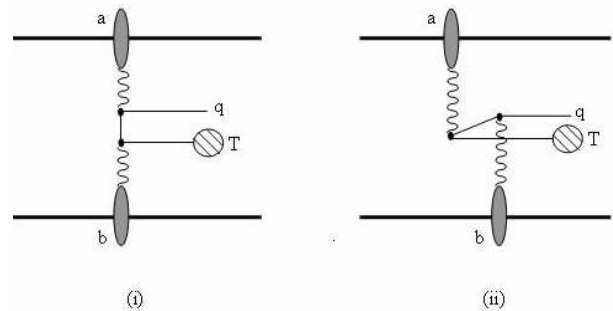


FIG. 1: Lowest-order Feynman diagrams for the pair production of a bound-free electron-positron pair in heavy-ion collisions: (i) *direct* and (ii) *crossed* diagrams for the simultaneous capture of the electron into a bound state of target (T) ion. In the figure,  $a$  and  $b$  represents the two ions, and  $\mathbf{q}$  is the momentum of the positron [9].

approximation, the pair creation with simultaneous capture of the electron by one of the ions is then described by convoluting the electron line in Fig. 1 with the momentum wave function of the final bound state [9]. In the following, we consider the collision of the ions in the ‘collider frame’ with zero total momentum of the overall system. In these coordinates, the two nonzero components of the vector potential of ion  $a$  is given by

$$A_a^0 = -[2\pi Ze] \delta(q_0') e^{[-i\mathbf{q}_\perp \cdot \frac{\mathbf{b}}{2}]} \int_{-\infty}^{\infty} d^3\mathbf{r} \frac{e^{-i\mathbf{q}' \cdot \mathbf{r}}}{|\mathbf{r}|} \quad (4a)$$

$$A_a^z = \beta A_a^0, \quad (4b)$$

while, similarly, the potential of ion  $b$  is obtained by just substituting the impact parameter  $b \rightarrow -b$  in the exponent of Eq. (4a) and the relative velocity  $\beta \equiv \frac{v}{c} \rightarrow -\beta$  in the formulas above. In these expressions, moreover,  $v$  refers the velocity of nucleus  $a$  moving from right to left parallel to the  $z$  axis. Nucleus  $b$  moves from left to right with velocity  $-v$ . In this work, we consider only the symmetric collisions (equal mass and equal charge) of the heavy ions, although the calculations can be done easily for the asymmetric collisions. For the overall collision system, therefore, the classical four-potential  $A^\mu$  can be written as [11, 12]:

$$A^\mu = A_a^\mu + A_b^\mu \quad (5)$$

which describe a retarded Lienard-Wiechert interactions.

To evaluate the diagrams in Fig. 1, we need of course a proper set of one-particle states in order to represent the electron-positron pairs after their generation in the field of the moving ions. For the outgoing positron, the spinor structure is

$$\mathbf{u}_{\sigma_q}^{(+)} = \sqrt{\frac{E_q^{(+)} + mc^2}{2mc^2}} \left[ \begin{array}{c} \phi^{(s)} \\ \frac{\boldsymbol{\sigma} \cdot \mathbf{p} c}{E_q^{(+)} + mc^2} \phi^{(s)} \end{array} \right] \quad (6)$$

(for spinors with positive energy  $E_q^{(+)} > 0$ ), and where  $\phi^{(s)} = \chi_{1/2}^{(s)}$  denotes a Pauli spinor and  $s = \pm 1/2$  its spin projection. Here, after the creation of electron-positron pairs, electron is captured by one of the colliding ions and positron becomes free which is described by the plane-waves

$$\Psi_q^{(+)} = N_+ \left[ e^{i\mathbf{q}\cdot\mathbf{r}} \mathbf{u}_{\sigma_q}^{(+)} + \Psi' \right], \quad (7)$$

and together with the (correction) term  $\Psi'$  in order to account for the distortion due to the charge of one of the nucleus. In expression (7), moreover,

$$N_+ = e^{-\pi a_+/2} \Gamma(1 + ia_+), \quad a_+ = \frac{Ze^2}{v_+}, \quad (8)$$

is a normalization constant which accounts for the distortion of the wave function is acceptable for  $Z\alpha \ll 1$  [6, 13, 14], and where  $\alpha = e^2/\hbar c \cong 1/137$  is the fine structure constant and  $v_+$  the velocity of the positron in the rest frame of the ion, into which the electron is captured in course of process (1). For sufficiently large energies of the ions, we can approximate  $v_+ \cong c = 1$  by

using natural units ( $\hbar = c = m = 1$ ), and which are used throughout this work if not stated otherwise.

After the pair production (1) has occurred, the electron is captured by one of the ions and, thus, need to be described as a bound state. In a semi-relativistic approximation, these electron states are often represented by [15, 16]

$$\Psi^{(-)} = \left( 1 - \frac{i}{2m} \boldsymbol{\alpha} \cdot \boldsymbol{\nabla} \right) \mathbf{u} \Psi_{\text{non-rel}}(r), \quad (9)$$

i.e. in terms of the non-relativistic (ground) state function

$$\Psi_{\text{non-rel}}(r) = \frac{1}{\sqrt{\pi}} \left( \frac{Z}{a_H} \right)^{3/2} e^{-Zr/a_H}, \quad (10)$$

of the hydrogen-like ion, and where  $\mathbf{u}$  represents the spinor part of the captured electron and  $a_H = 1/e^2$  the Bohr radius of atomic hydrogen.

Using the positron and electron states from above, the direct diagram in Fig. 1(i) can be written as:

$$\begin{aligned} \langle \Psi^{(-)} | S_{ab} | \Psi_q^{(+)} \rangle &= i \sum_p \sum_s \int_{-\infty}^{\infty} \frac{d\omega}{2\pi} \frac{\langle \Psi^{(-)} | V_a(\omega - E^{(-)}) | \chi_p^{(s)} \rangle \langle \chi_p^{(s)} | V_b(E_q^{(+)} - \omega) | \Psi_q^{(+)} \rangle}{(E_p^{(s)} - \omega)} \\ &= i \sum_p \sum_s \int_{-\infty}^{\infty} \frac{d\omega}{2\pi} \int_{-\infty}^{\infty} d^3\mathbf{r} \left( 1 + \frac{i}{2m} \boldsymbol{\alpha} \cdot \boldsymbol{\nabla} \right) \Psi_{\text{non-rel}}(r) e^{i\mathbf{p}\cdot\mathbf{r}} A_a(\mathbf{r}; \omega - E^{(-)}) \\ &\quad \times \int_{-\infty}^{\infty} d^3\mathbf{r}' N_+ e^{-i(\mathbf{p}-\mathbf{q})\cdot\mathbf{r}'} A_b(\mathbf{r}'; E_q^{(+)} - \omega) \frac{\langle \mathbf{u} | (1 - \beta\alpha_z) | \mathbf{u}_{\sigma_p}^{(s)} \rangle \langle \mathbf{u}_{\sigma_p}^{(s)} | (1 + \beta\alpha_z) | \mathbf{u}_{\sigma_q}^{(+)} \rangle}{(E_p^{(s)} - \omega)}, \quad (11) \end{aligned}$$

and where  $V_a$  and  $V_b$  are the potentials of the two nuclei  $a$  and  $b$ ,

$$V_a = (1 - \beta\alpha_z) A_a^0 \quad (13a)$$

$$V_b = (1 + \beta\alpha_z) A_b^0, \quad (13b)$$

respectively, and with the vector potentials taken from above [cf. Eq. 4]. Apparently, therefore, the overall (direct) amplitude contains a three-fold integration over the coordinates of the bound electron ( $d^3\mathbf{r}$ ), the coordinates of the free positron ( $d^3\mathbf{r}'$ ) as well as the integration over the frequency  $\omega$  of the virtually exchanged photons between the heavy ions. In the evaluation of Eq. (11), moreover, we have used the completeness relation

$$\sum_p \left| \langle \chi_p^{(+)} \rangle \langle \chi_p^{(+)} \right| + \left| \langle \chi_p^{(-)} \rangle \langle \chi_p^{(-)} \right| = 1 \quad (14)$$

with  $\chi_p^{(s)}$  being:

$$\chi_p^{(+)} = e^{i\mathbf{p}\cdot\mathbf{r}} \mathbf{u}_{\sigma_p}^{(+)} \quad (15a)$$

$$\chi_p^{(-)} = e^{-i\mathbf{p}\cdot\mathbf{r}} \mathbf{u}_{\sigma_p}^{(-)}. \quad (15b)$$

In this notation of the one-particle states, again,  $\mathbf{u}_{\sigma_p}^{(s)}$  refers to the spinor part of the intermediate state of  $\chi_p^{(s)}$ , and the summation over the spin and momentum of the one particle can be replaced by

$$\sum_p = \sum_{\sigma_p} \sum_{\mathbf{p}} \rightarrow \sum_{\sigma_p} \int \frac{d^3\mathbf{p}}{(2\pi)^3}. \quad (16)$$

We can perform the integration over  $\mathbf{r}$  and  $\mathbf{r}'$  explicitly in Eq. (12). If we first consider the integral over  $\mathbf{r}$ , the two parts of this integral

$$\begin{aligned}
& \int_{-\infty}^{\infty} d^3\mathbf{r} \left( 1 + \frac{i}{2m} \boldsymbol{\alpha} \cdot \boldsymbol{\nabla} \right) \Psi_{\text{non-rel}}(r) e^{i\mathbf{p}\cdot\mathbf{r}} A_a(\mathbf{r}; \omega - E^{(-)}) \\
&= \int_{-\infty}^{\infty} d^3\mathbf{r} \Psi_{\text{non-rel}}(r) e^{i\mathbf{p}\cdot\mathbf{r}} A_a(\mathbf{r}; \omega - E^{(-)}) + \left( \frac{i}{2m} \right) \int_{-\infty}^{\infty} d^3\mathbf{r} \boldsymbol{\alpha} \cdot \boldsymbol{\nabla} \Psi_{\text{non-rel}}(r) e^{i\mathbf{p}\cdot\mathbf{r}} A_a(\mathbf{r}; \omega - E^{(-)}) \quad (17)
\end{aligned}$$

can be analyzed independently. Making use of the explicit form of the non-relativistic 1s-function  $\Psi_{\text{non-rel}}(r)$  and the vector potential  $A_a(\mathbf{r}; \omega - E^{(-)})$ , we can write the first part (on the rhs) of Eq. (17) as

$$\begin{aligned}
\int_{-\infty}^{\infty} d^3\mathbf{r} \Psi_{\text{non-rel}}(r) e^{i\mathbf{p}\cdot\mathbf{r}} A_a(\mathbf{r}; \omega - E^{(-)}) &= -[2\pi Z e] \delta(p'_0) e^{[-ip'_y \frac{b}{2}]} \frac{1}{\sqrt{\pi}} \left( \frac{Z}{a_H} \right)^{3/2} \int_{-\infty}^{\infty} d^3\mathbf{r} e^{-Zr/a_H} \frac{e^{i\mathbf{p}\cdot\mathbf{r}}}{\mathbf{r}} \\
&= -\frac{8\pi^2 Z e}{\sqrt{\pi}} \left( \frac{Z}{a_H} \right)^{3/2} \frac{e^{[i\mathbf{p}_{\perp} \cdot \frac{b}{2}]}}{\left( \frac{Z^2}{a_H^2} + \frac{p_z^2}{\gamma^2} + \mathbf{p}_{\perp}^2 \right)} \delta(\omega - E^{(-)} - \beta p_z). \quad (18)
\end{aligned}$$

Here, in the second line, we made use of the known integral

$$\int_{-\infty}^{\infty} d^3\mathbf{r} e^{-Zr/a_H} \frac{e^{i\mathbf{p}\cdot\mathbf{r}}}{\mathbf{r}} = \frac{4\pi}{\left( \frac{Z^2}{a_H^2} + \mathbf{p}^2 \right)} \quad (19)$$

together with the Lorentz transformation as displayed in

Appendix A. In Eq. (18), moreover,  $p_0$  represents the energy term,  $p_z$  the longitudinal momentum and,  $p_{\perp}$  ( $p_y$ ) is the transverse momentum of the intermediate state as given by Eq. (14).

The second part of the integral (17)

$$\begin{aligned}
& \left( \frac{i}{2m} \right) \int_{-\infty}^{\infty} d^3\mathbf{r} \boldsymbol{\alpha} \cdot \boldsymbol{\nabla} \Psi_{\text{non-rel}}(r) e^{i\mathbf{p}\cdot\mathbf{r}} A_a(\mathbf{r}; \omega - E^{(-)}) \\
&= \left( \frac{i}{2m} \right) \frac{1}{\sqrt{\pi}} \left( \frac{Z}{a_H} \right)^{3/2} \left\{ -[2\pi Z e] \delta(p'_0) e^{[-ip'_y \frac{b}{2}]} \int_{-\infty}^{\infty} d^3\mathbf{r} \boldsymbol{\alpha} \cdot \boldsymbol{\nabla} e^{-Zr/a_H} \frac{e^{i\mathbf{p}\cdot\mathbf{r}}}{\mathbf{r}} \right\} \\
&= -\frac{1}{2m} \frac{1}{\sqrt{\pi}} \left( \frac{Z}{a_H} \right)^{3/2} 8\pi^2 Z e \boldsymbol{\alpha} \cdot \mathbf{p} \delta(\omega - E^{(-)} - \beta p_z) \frac{e^{[i\mathbf{p}_{\perp} \cdot \frac{b}{2}]}}{\left( \frac{Z^2}{a_H^2} + \frac{p_z^2}{\gamma^2} + \mathbf{p}_{\perp}^2 \right)} \quad (20)
\end{aligned}$$

can be evaluated by following similar lines, but it now contains the factor  $\frac{i}{2m} \boldsymbol{\alpha} \cdot \boldsymbol{\nabla}$  which arises from the wave function of the captured electron. This additional ‘derivative’ with regard to the coordinates of the electrons can be removed by an integration by parts,

$$\int_{-\infty}^{\infty} d^3\mathbf{r} \boldsymbol{\alpha} \cdot \boldsymbol{\nabla} e^{-Zr/a_H} \frac{e^{i\mathbf{p}\cdot\mathbf{r}}}{\mathbf{r}} = -i\boldsymbol{\alpha} \cdot \mathbf{p} \frac{4\pi}{\left( \frac{Z^2}{a_H^2} + \mathbf{p}^2 \right)}. \quad (21)$$

For the overall integral (17), this gives rise to the expression:

$$\begin{aligned}
& \int_{-\infty}^{\infty} d^3\mathbf{r} \left( 1 + \frac{i}{2m} \boldsymbol{\alpha} \cdot \boldsymbol{\nabla} \right) \Psi_{\text{non-rel}}(r) e^{i\mathbf{p}\cdot\mathbf{r}} A_a(\mathbf{r}; \omega - E^{(-)}) \\
&= - \left[ 1 + \frac{\boldsymbol{\alpha} \cdot \mathbf{p}}{2m} \right] 8\pi^2 Z e \frac{1}{\sqrt{\pi}} \left( \frac{Z}{a_H} \right)^{3/2} \frac{\delta(\omega - E^{(-)} - \beta p_z)}{\left( \frac{Z^2}{a_H^2} + \frac{p_z^2}{\gamma^2} + \mathbf{p}_{\perp}^2 \right)} e^{[i\mathbf{p}_{\perp} \cdot \frac{b}{2}]}, \quad (22)
\end{aligned}$$

where  $E^{(-)}$  is the energy of the captured electron.

Using analogue steps, the integral over  $\mathbf{r}'$  in Eq. (12) can be written as:

$$\int_{-\infty}^{\infty} d^3\mathbf{r}' N_+ e^{-i(\mathbf{p}-\mathbf{q})\cdot\mathbf{r}'} A_b(\mathbf{r}'; E_q^{(+)} - \omega) = -N_+ 8\pi^2 Z e \gamma^2 \frac{\delta(E_q^{(+)} - \omega - \beta(p_z - q_z))}{(p_z - q_z)^2 + \gamma^2(\mathbf{p}_\perp - \mathbf{q}_\perp)^2} e^{i(\mathbf{p}_\perp - \mathbf{q}_\perp)\cdot\frac{\mathbf{b}}{2}}, \quad (23)$$

where  $E_q^{(+)}$  is now the energy of the positron. Thus, by combining both integrals in Eq. (17), we obtain for the direct BFPP amplitude the explicit expression:

$$\begin{aligned} \langle \Psi^{(-)} | S_{ab} | \Psi_q^{(+)} \rangle &= iN_+ \sum_s \sum_{\sigma_p} \int \frac{d^3\mathbf{p}}{(2\pi)^3} \int \frac{d\omega}{2\pi} e^{i(\mathbf{p}_\perp - \frac{\mathbf{q}_\perp}{2})\cdot\mathbf{b}} 8\pi^2 Z e \frac{1}{\sqrt{\pi}} \left( \frac{Z}{a_H} \right)^{3/2} \frac{\delta(\omega - E^{(-)} - \beta p_z)}{\left( \frac{Z^2}{a_H^2} + \frac{p_z^2}{\gamma^2} + \mathbf{p}_\perp^2 \right)} \left[ 1 + \frac{\boldsymbol{\alpha} \cdot \mathbf{p}}{2m} \right] \\ &\times 8\pi^2 Z e \gamma^2 \frac{\delta(E_q^{(+)} - \omega - \beta(p_z - q_z))}{(p_z - q_z)^2 + \gamma^2(\mathbf{p}_\perp - \mathbf{q}_\perp)^2} \frac{\langle \mathbf{u} | (1 - \beta\alpha_z) | \mathbf{u}_{\sigma_p}^{(s)} \rangle \langle \mathbf{u}_{\sigma_p}^{(s)} | (1 + \beta\alpha_z) | \mathbf{u}_{\sigma_q}^{(+)} \rangle}{E_p^{(s)} - \omega}, \end{aligned} \quad (24)$$

and where  $E_p^{(s)}$  is the energy of intermediate state.

The vector  $\mathbf{p}$  describes the momentum of the intermediate (electron and positron) states in the field of the ion and can be decomposed into its transverse and parallel part,  $\mathbf{p} = \mathbf{p}_\perp + p_z$ , relative to the motion of the ions. In Eq. 24, the two Dirac delta functions gives us the component along the velocity of the heavy ions

$$p_z = \frac{E_q^{(+)} - E^{(-)} + \beta q_z}{2\beta}, \quad (25a)$$

in terms of the energies and the longitudinal momentum,  $q_z$ , of the positron. Similarly, we can write the frequency of virtually exchanged photons as

$$\omega = E^{(-)} + \beta p_z = \frac{E^{(-)} + E_q^{(+)} + \beta q_z}{2}, \quad (25b)$$

owing to the conservation of the momentum that is obtained from the Dirac delta functions in Eq. (24). In contrast to the parallel part, however, the transverse momentum of the electrons  $\mathbf{p}_\perp$  is not fixed by the kinematics of the collision partners, but also depends on the momentum that is carried by the fields. After integrating the Eq. (24) over  $\omega$  and  $p_z$ , and by inserting the values from Eqs. (25) into Eq. (24), the transition matrix element for a fixed spin and momentum state of the positron as well as for a given intermediate state can be expressed as

$$\langle \Psi^{(-)} | S_{ab} | \Psi_q^{(+)} \rangle = \frac{iN_+}{2\beta} \frac{1}{\sqrt{\pi}} \left( \frac{Z}{a_H} \right)^{3/2} \int \frac{d^2 p_\perp}{(2\pi)^2} e^{i(\mathbf{p}_\perp - \frac{\mathbf{q}_\perp}{2})\cdot\mathbf{b}} F(-\mathbf{p}_\perp : \omega_a) F(\mathbf{p}_\perp - \mathbf{q}_\perp : \omega_b) \mathcal{T}_q(\mathbf{p}_\perp : +\beta), \quad (26)$$

where  $\mathbf{b}$  is again the impact parameter of the ion-ion collision, and the function  $F(q, \omega)$  can be described as the scalar part of the field associated with the ions  $a$  and  $b$  in momentum space. Explicit form of these scalar fields can be written in terms of the corresponding frequencies as

$$F(-\mathbf{p}_\perp : \omega_a) = \frac{4\pi Z e}{\left( \frac{Z^2}{a_H^2} + \frac{\omega_a^2}{\gamma^2 \beta^2} + \mathbf{p}_\perp^2 \right)} \quad (27a)$$

for the frequency  $\omega_a$ , and as

$$F(\mathbf{p}_\perp - \mathbf{q}_\perp : \omega_b) = \frac{4\pi Z e \gamma^2 \beta^2}{(\omega_b^2 + \gamma^2 \beta^2 (\mathbf{p}_\perp - \mathbf{q}_\perp)^2)} \quad (27b)$$

for the frequency  $\omega_b$ , respectively.

Owing to the asymmetry in the behavior of the electrons and positrons in course of the BFPP process, the wave functions of the free positron and captured electron will differ substantially. This difference gives rise also to different expressions for the frequencies of the virtual photons as emitted by the two nuclei, i.e.

$$\omega_a = \frac{-E^{(-)} + E_q^{(+)} + \beta q_z}{2} = \beta p_z, \quad (28a)$$

for ion  $a$ , and

$$\omega_b = \frac{E_q^{(+)} - E^{(-)} - \beta q_z}{2} = \beta(p_z - q_z). \quad (28b)$$

for ion  $b$ , respectively. As mentioned before, these frequencies are obtained from integrating Eq. (24). Apart

from the scalar field of each ion, Eq. (26) contains also the transition amplitudes  $\mathcal{T}$  which relates the intermediate photon lines to the outgoing electron-positron lines. This amplitude depends explicitly on the (relative) velocity of the ions  $\beta$ , the transverse momentum  $\mathbf{p}_\perp$ , and the momentum of the positron  $q$ , and it is given by

$$\begin{aligned} \mathcal{T}_q(\mathbf{p}_\perp : +\beta) &= \sum_s \sum_{\sigma_p} \frac{1}{\left(E_p^{(s)} - \left(\frac{E^{(-)} + E_q^{(+)}}{2}\right) - \beta \frac{q_z}{2}\right)} \left[1 + \frac{\boldsymbol{\alpha} \cdot \mathbf{p}}{2m}\right] \\ &\times \left\langle \mathbf{u} | (1 - \beta \alpha_z) | \mathbf{u}_{\sigma_p}^{(s)} \right\rangle \left\langle \mathbf{u}_{\sigma_p}^{(s)} | (1 + \beta \alpha_z) | \mathbf{u}_{\sigma_q}^{(+)} \right\rangle. \end{aligned} \quad (29)$$

In this amplitude, moreover, the parallel component of the intermediate state momentum  $p_z$  is determined by Eq. (25a). Finally, let us note that the integration

over the impact parameter  $b$  in Eq. (26) can be carried out also analytically. Following very similar lines, it is possible also to evaluate the *crossed*-term amplitude  $\left\langle \Psi^{(-)} | S_{ba} | \Psi_q^{(+)} \right\rangle$  from Fig. 1.

Having the amplitudes for the *direct* and *crossed* diagram, we are now prepared to write down the cross section for the generation of a free-bound electron-positron pair in collisions of two heavy ions

$$\sigma = \int d^2b \sum_{q < 0} \left| \left\langle \Psi^{(-)} | S | \Psi_q^{(+)} \right\rangle \right|^2, \quad (30)$$

where  $S = S_{ab} + S_{ba}$  denotes the sum of the *direct* and *crossed* terms in Fig. 1. Making use of all the simplifications from above, these cross sections for the BFPP can be expressed as:

$$\begin{aligned} \sigma &= \int d^2b \sum_{q < 0} \left| \left\langle \Psi^{(-)} | S_{ab} | \Psi_q^{(+)} \right\rangle + \left\langle \Psi^{(-)} | S_{ba} | \Psi_q^{(+)} \right\rangle \right|^2 \\ &= \frac{|N_+|^2}{4\beta^2} \frac{1}{\pi} \left(\frac{Z}{a_H}\right)^3 \sum_{\sigma_q} \int \frac{d^3q d^2p_\perp}{(2\pi)^5} \left( \mathcal{A}^{(+)}(q : \mathbf{p}_\perp) + \mathcal{A}^{(-)}(q : \mathbf{q}_\perp - \mathbf{p}_\perp) \right)^2, \end{aligned} \quad (31)$$

with

$$\mathcal{A}^{(+)}(q : \mathbf{p}_\perp) = F(-\mathbf{p}_\perp : \omega_a) F(\mathbf{p}_\perp - \mathbf{q}_\perp : \omega_b) \mathcal{T}_q(\mathbf{p}_\perp : +\beta), \quad (32a)$$

and

$$\mathcal{A}^{(-)}(q : \mathbf{q}_\perp - \mathbf{p}_\perp) = F(\mathbf{p}_\perp - \mathbf{q}_\perp : \omega_b) F(-\mathbf{p}_\perp : \omega_a) \mathcal{T}_q(\mathbf{q}_\perp - \mathbf{p}_\perp : -\beta). \quad (32b)$$

being some proper products of the transition amplitudes and scalar parts of the fields as associated with ions  $a$  and  $b$ . All these functions have been displayed explicitly in Eqs. (27) and (29) above. Moreover, the square of the normalization constant for the positron wave function is equal to [6, 13]

$$|N_+|^2 = \frac{2\pi a_+}{e^{2\pi a_+} - 1}. \quad (33)$$

Indeed, this constant appears to be very similar to

$$\frac{2\pi\alpha Z}{e^{2\pi\alpha Z} - 1}, \quad (34)$$

i.e. the factor that represents the distortion of the positron wave function due to the shielding of the nucleus by the electron [13, 14, 17].

### III. RESULTS AND DISCUSSIONS

Calculations have been performed for the total production cross sections of bound-free electron-positron pairs in relativistic collisions of bare ions. Theoretical cross sections are obtained especially for the collisions of  $Au + Au$  ions at energies relevant for the RHIC facility as well as for  $Pb + Pb$  ions at LHC energies. These cross sections are compared with those for the production of free electron-positron pairs. While, however, the

TABLE I: Bound-free pair production cross sections  $\sigma_{\text{BFPP}}$  (in barn) for selected collision systems and cross sections as accessible at RHIC and LHC collider facilities.

		This work Ref. [18]	
RHIC	$Au + Au$ at 100 GeV	94.5	94.9
LHC	$Pb + Pb$ at 2957 GeV	202	225

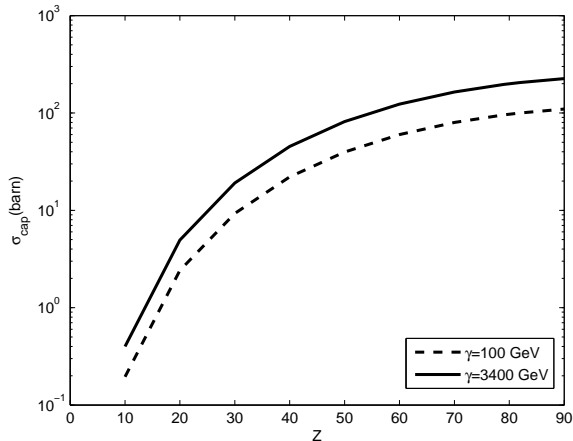


FIG. 2: BFPP cross sections for two different systems as functions of the nuclear charge  $Z$ . BFPP cross sections (in barn) for the symmetric collision of bare ions with nuclear charge  $Z$  at 100 GeV/nucleon (dashed line) and 3400 GeV/nucleon (solid line). The capture cross sections increases by about 3 order of magnitude in going from  $Z = 10$  to  $Z = 90$ .

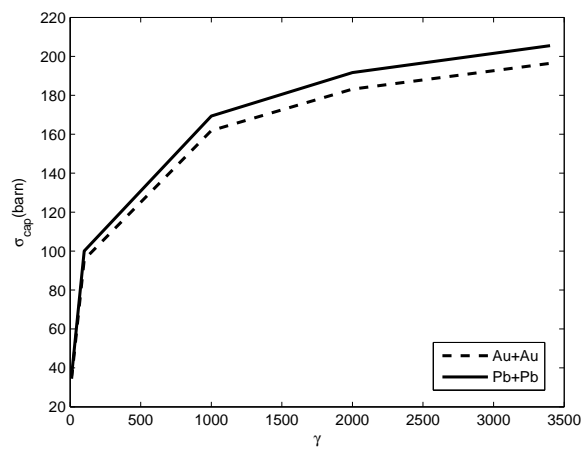


FIG. 3: BFPP cross sections for two different systems ( $Au + Au$ -dashed line and  $Pb + Pb$ -solid line) as functions of the  $\gamma$ . The magnitude of  $\gamma$  is going from 10 to 3400.

free-pair production includes an eight dimensional integral, the BFPP cross sections eventually depend only on five-dimensional integrals. To evaluate these amplitudes, Monte-Carlo techniques were utilized, and the integrands have been tested on about 10 million randomly chosen ‘positions’ in order to ensure a sufficient convergence of our theoretical results. The total numerical errors in the computations is estimated to be less or approximately five percent.

As a test of our implementation, first computations of the total BFPP cross sections were performed for a few selected collision energies. Table I displays these BFPP cross sections for the two collision systems from

above and for those collision energies that are relevant for forthcoming experiments at the RHIC and LHC collider facilities. Our results for the total cross sections are in good-to-excellent agreement with the previous computations by Meier *et al.* [18], especially for the RHIC energies of 100 GeV per nucleon. For the much higher collision energies of  $\sim 3000$  GeV per nucleon, that will be available at the LHC storage ring, our theoretical predictions for the BFPP cross sections are in contrast lower by about 20 %, compared with the computations by Meier and coworkers.

As mentioned above, the correction term  $\Psi'$  was omitted to the positron wave functions in Eq. (7), in line with previous experience and computations of the free (electron-positron) pair production for which a perfect agreement with experiment was found by omitting this term [11, 12]. We therefore conclude that the distortion of the positron states due to the shielding of the electron is small and remains negligible for the present computations.

To understand the importance of the bound-free process, Fig. 2 displays the BFPP cross sections for symmetric collisions of ions with charge  $Z$  as function of the nuclear charge. Cross sections are shown for the two collision energies  $E = 100$  GeV/nucleon (dashed line) and 3400 GeV/nucleon (solid line) as important for modern accelerators. While the cross sections for the production of free pair scale approximately with  $\approx (Z\alpha)^4 \ln^3(\gamma)$ , the BFPP cross sections increase with  $\approx (Z\alpha)^8 \ln(\gamma)$ . In this scaling behavior, the reason for an extra factor  $Z^3$  arises from the bound wave function of the electron, while another power in  $Z$  comes from the normalization constant for the positron wave function.

Fig. 3 shows the total BFPP cross sections for two different systems as functions of the Lorentz contraction factor  $\gamma$ . Our calculation is done in the center-of-momentum frame, therefore the relationship between the Lorentz factor  $\gamma$  and the collider energy per nucleon in GeV  $E/A$  is given by  $\gamma = 1/\sqrt{1-v^2} = E/m_0$ , where  $m_0$  is the mass of the nucleons. Results are displayed for  $Pb + Pb$  collisions (solid line) and for  $Au + Au$  collisions (dashed line). As function of the Lorentz factor  $\gamma$ , the free pair production scales with  $\ln^3(\gamma)$  and the bound-free pair production with  $\ln(\gamma)$ . All these results are obtained in previous computations [6, 13, 19, 20] and, thus, we also verify that our calculations gives the similar results.

Results for the free and bound-free pair production are displayed in the figures 4 to 7 within the same graph. At collision energies of 100 GeV per nucleon, as relevant to the RHIC facility, we have considered  $Au + Au$  collisions, while  $Pb + Pb$  collisions were analyzed at 3400 GeV per nucleon, as they are hoped to be reached within the near future with the LHC at CERN. The same notation is used throughout the figures 4 to 7. Thin-lines and thin-dashed lines represent the bound-free pair production and free-pair production at RHIC collisions of  $Au + Au$ , respectively. On the other hand, thick lines and thick-dashed lines shows the BFPP and free pair production at LHC

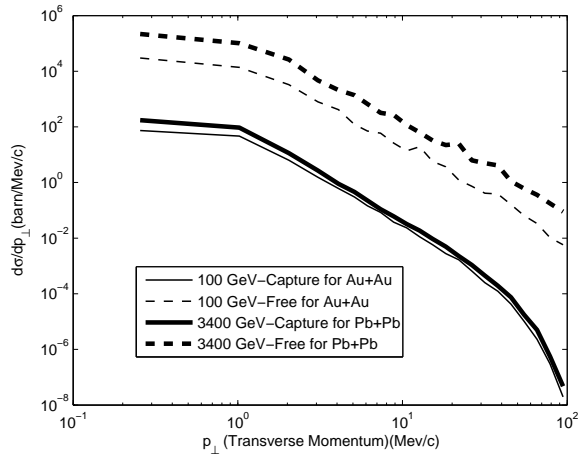


FIG. 4: The differential cross section as function of the transverse momentum ( $p_{\perp}$ ) of the produced positrons is shown in the graph. Calculated differential cross sections are shown for the two collision systems  $Au + Au$  at 100 GeV per nucleon and  $Pb + Pb$  at 3400 GeV per nucleon, respectively. When compared with the production of free electron-positron pairs, the BFPP cross section for the capture of the electron into the  $1s$  ground state is suppressed by about three orders of magnitude for all transverse momenta between 0.1 and 100 MeV/c.

collisions of  $Pb + Pb$  respectively.

Fig. 4 plots the the differential cross section as function of the transverse momentum of the produced positrons. From this figure, it becomes clear that the bound-free and free pair production distributions display a rather similar behavior as function of transverse momentum, although the free-pair distribution function is larger by about 3 orders of magnitude than the BFPP function. Obviously, moreover, BFPP distribution function decreases much faster with the size of the transverse momentum than those for the free-pair production.

Figs. 5 and 6 displays the differential cross sections as function of the longitudinal momentum and the energy, respectively. Again, cross sections are shown for the free and bound-free case. From Fig. 5 we find that the ratio of the RHIC and LHC increases if the value of the longitudinal momentum increases. Moreover, since the longitudinal momentum of the positron is much higher than the transverse momentum, the energy of the produced positron arises mainly from the longitudinal momentum of the positrons. Therefore, the behavior of the differential cross section as functions of longitudinal momentum and energy must look very similar as seen from Figs. 5 and 6. We can conclude that energy of the positrons,  $E = \sqrt{p_{\perp}^2 + p_z^2 + 1}$ , consist of mainly by the longitudinal momentum of the positrons.

Finally, Fig.7 plots the differential cross section as function of the rapidity. At RHIC energies, the behavior of the free and bound-free differential cross sections of rapidity is almost the same, while a different behavior

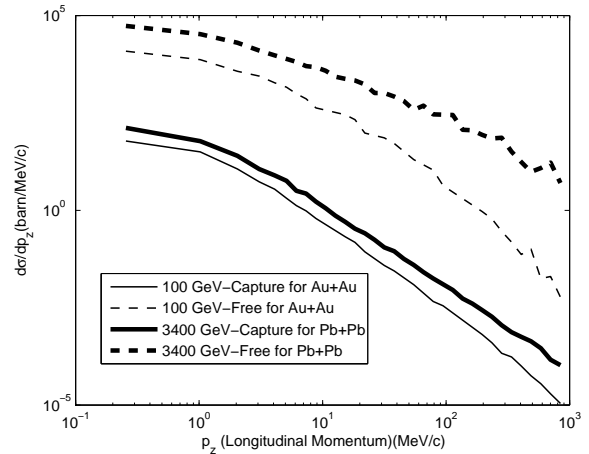


FIG. 5: The differential cross section is shown as function of the longitudinal momentum ( $p_z$ ) of the produced positrons. The notations are the same as in Fig. 4.

is observed at LHC energies. For large values of the rapidity, the bound-free cross sections decay more rapidly than for the free production sections. Since the rapidity is a function of the energy and momenta,

$$y = \frac{1}{2} \ln \left[ \frac{p_0 + p_z}{p_0 - p_z} \right], \quad (35)$$

the discrepancies in the behavior in the cross sections as function of the longitudinal momenta and the energies appears closely related to its the behavior as function of the rapidity.

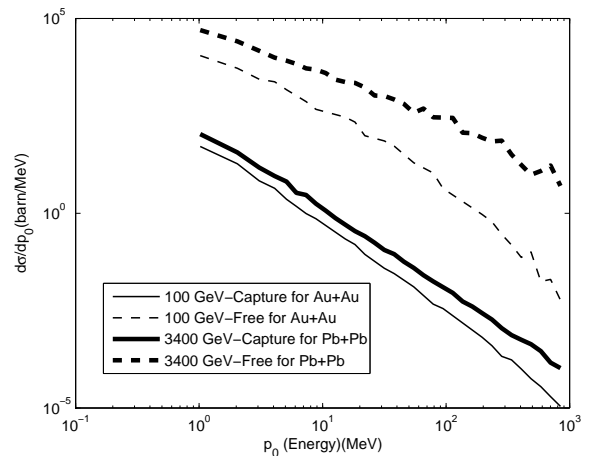


FIG. 6: The differential cross section as function of the energy ( $p_0$ ) of the produced positrons is shown in the graph. The notations are the same as in Fig. 4.



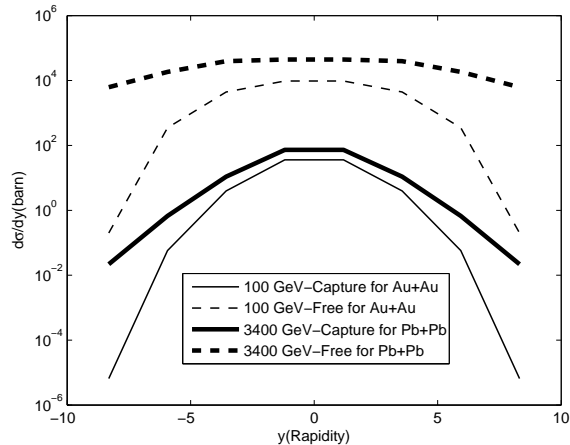


FIG. 7: The differential cross section is shown as function of the rapidity ( $y$ ). The notations are the same as in Fig. 4.

#### IV. CONCLUDING REMARKS

In this work, we have investigated the electron-positron pair production that is associated with the (simultaneous) capture of the electron into the  $K$ -shell of one of the ions. Calculations of the cross sections have been performed especially for two collision systems,  $Au + Au$  and  $Pb + Pb$ , and for energies that are relevant for the RHIC and LHC facilities. In the framework of QED perturbation theory, the lowest-order Feynman diagrams have been evaluated by applying Darwin wave functions for the  $1s$  bound state of the electron and Sommerfeld-Maue wave functions for the continuum states of the outgoing positron. In line with previous experience, however, we have not taken into account the correction term for the positron wave function whose influence was estimated to be small. We plan to incorporate this term in the future to analyze its contribution in further detail.

Comparison of our theoretical cross sections is made with previous computations as far as available. Good agreement is found especially for the total cross sections of  $Au + Au$  collisions at 100 GeV per nucleon as utilized at RHIC. For these collision, it is found in particular that the free and bound-free pair production cross section behave very similar as a function of energy with an almost constant factor of  $\sim 10^3$  with which the bound-free pair production is suppressed. This is quite different for collision at  $\gtrsim 3000$  GeV/nucleon, the expected conditions at the LHC, where there is discrepancy between BFPP and free pair production differential cross sections especially for large values of longitudinal momentum, energy and rapidity.

For the total electron-positron pair production, the effect of the ‘Coulomb correction’ is known to play an important role [21] due to multi-photon exchange of the produced electron-positron with the colliding nuclei. This Coulomb correction for the free pair production has a

negative value and it is proportional to  $Z^2$  which is obtained by Bethe-Maximon [22]. So far, these higher-order corrections were not included in the computation but we plan to derive and calculate this effect in a forthcoming work.

#### Acknowledgments

This research is partially supported by the Istanbul Technical University and Kadir Has University. We personally thank S. R. Klein and G. Baur for valuable advise in calculating the cross sections and M. Şengül for the carefully reading of our article.

#### APPENDIX A: LORENTZ TRANSFORMATION OF THE 4-VECTOR POTENTIAL

In Section II, the integrals (18 and 20) were evaluated by using the Lorentz-transformed potentials of the Coulomb field of the heavy ions. Here, we derive this potential in momentum space and perform the Lorentz transformation onto it. In the rest frame of an ion with the nuclear charge  $Z$ , fixed to the coordinates  $(0, b/2, 0)$ , the four-vector potential is given by:

$$\begin{aligned} \mathbf{A}' &= 0 \\ A'_0 &= \frac{-Ze}{[x'^2 + (y' - b/2)^2 + z'^2]^{1/2}}. \end{aligned} \quad (\text{A1})$$

In momentum space, this vector potential can be expressed by

$$\begin{aligned} A'_0(q') &= \int d^4x' e^{iq' \cdot x'} A'_0(x') \\ &= -[2\pi Ze] \delta(q'_0) e^{[-iq'_y \frac{b}{2}]} \\ &\quad \times \int_{-\infty}^{\infty} d^3\mathbf{r}' \frac{e^{-i\mathbf{q}' \cdot \mathbf{r}'}}{|\mathbf{r}'|}, \end{aligned} \quad (\text{A2})$$

and with

$$\mathbf{r}' = \mathbf{x}' + (\mathbf{y}' - \mathbf{b}'/2) + \mathbf{z}'. \quad (\text{A3})$$

Moreover, since  $\mathbf{A}' = 0$  and  $A'_\mu$  must transforms like a four-vector, we obtain

$$\begin{aligned} A_0(q) &= \gamma(A'_0 - \beta A'_1) = \gamma A'_0 \\ A_1(q) &= \gamma(A'_1 - \beta A'_0) = -\gamma \beta A'_0 \\ \mathbf{A}_\perp &= \mathbf{A}'_\perp = 0. \end{aligned} \quad (\text{A4})$$

Thus, by doing the integration over  $\mathbf{r}'$  on the rhs of Eq. (A2) and by performing the Lorentz transformations, we obtain the potential for the colliding ions:

$$A_0 = -[8\pi^2 Ze] \delta(q_0 + \beta q_1) \gamma^2 \frac{e^{-i\mathbf{q}_\perp \cdot \mathbf{b}/2}}{[q_1^2 + \gamma^2 \mathbf{q}_\perp^2]}, \quad (\text{A5})$$

and where  $q_{\parallel}$  refers to the longitudinal momentum,  $\mathbf{q}_{\perp}$  the transverse momentum and  $q_0$  is the energy term.

- 
- [1] R. Bruce, J.M. Jowett, S. Gilardoni, A. Drees, W. Fischer, S. Tepikian and S.R. Klein, Phys. Rev. Lett. **99**, 144801 (2007).
- [2] S.R. Klein, Nucl. Instr. Meth. A **459**, 51 (2001).
- [3] A. Belkacem, H. Gould, B. Feinberg, R. Bossingham and W.E. Meyerhof, Phys. Rev. Lett. **71**, 1514 (1993).
- [4] H.F. Krause, C.R. Vane, S. Datz, P. Grafström, H. Knudsen, C. Scheidenberger and R.H. Schuch, Phys. Rev. Lett. **80**, 1190 (1998).
- [5] A.J. Baltz, M.J. Rhoades-Brown and J. Weneser, Phys. Rev. A **50**, 4842 (1994).
- [6] C.A. Bertulani and G. Baur, Phys. Rep. **163**, 299 (1988).
- [7] A.J. Baltz, G. Baur, D. d'Enterria, L. Frankfurt, F. Gelis, V. Guzey, K. Hencken, Yu. Kharlov, M. Klasen, S.R. Klein, V. Nikulin, J. Nystrand, I.A. Pshenichnov, S. Sadovsky, E. Scapparone, J. Seger, M. Strikman, M. Tverskoy, R. Vogt, S.N. White, U.A. Wiedemann, P. Yepes, M. Zhalov, Phys. Rep. **458**, 1 (2008).
- [8] A. Aste, K. Hencken, D. Trautmann and G. Baur, Phys. Rev. A **50**, 3980 (1994).
- [9] M.J. Rhoades-Brown, C. Bottcher and M.R. Strayer, Phys. Rev. A **40**, 2831 (1989).
- [10] G. Baur, Phys. Rev. A **44**, 4767 (1991).
- [11] C. Bottcher and M.R. Strayer, Phys. Rev. D **39**, 1330 (1989).
- [12] M.C. Guclu, J.C. Wells, A.S. Umar, M.R. Strayer and D.J. Ernst, Phys. Rev. A **51**, 1836 (1995).
- [13] C.A. Bertulani and D. Dolci, Nucl. Phys. A **683**, 635 (2001).
- [14] A. Aste, Eur. Phys. Lett. **81**, 61001(2008).
- [15] V.B. Berestetskii, E.M. Lifshitz and L.P. Pitaevskii, Relativistic Quantum Field Theory (Pergamon Press, New York, 1979).
- [16] J. Eichler and W.E. Meyerhof, Relativistic Atomic Collisions (Academic Press, California, 1995).
- [17] J. Eichler, Phys. Rev. Lett. **75**, 3653 (1995).
- [18] H. Meier, Z. Halabuka, K. Hencken, D. Trautmann and G. Baur, Phys. Rev. A **63**, 032713 (2001).
- [19] C. A. Bertulani and G. Baur, Phys. Rev. D **58**, 034005 (1997).
- [20] H. Meier, Z. Halabuka, K. Hencken, D. Trautmann and G. Baur, Eur. Phys. J. C **5**, 287 (1998).
- [21] A.J. Baltz, Phys. Rev. Lett. **100**, 062302 (2008).
- [22] H.A. Bethe and L.C. Maximon, Phys. Rev. **93**, 768 (1954); Handel Davies, H.A. Bethe and L.C. Maximon, Phys. Rev. **93**, 788 (1954).